IEEE Access
Multidisciplinary ⋮ Rapid Review ⋮ Open Access Journal

Received 12 October 2023, accepted 8 November 2023, date of publication 13 November 2023,
date of current version 17 November 2023.

Digital Object Identifier 10.1109/ACCESS.2023.3332138

RESEARCH ARTICLE

Error Tracking-Based Neuro-Adaptive Learning Control for Pneumatic Artificial Muscle Systems With Output Constraint

GUANGMING ZHU[1,2] AND QIUZHEN YAN[2]
[1]College of Economics and Management, Zhejiang University of Water Resources and Electric Power, Hangzhou 310018, China
[2]College of Information Engineering, Zhejiang University of Water Resources and Electric Power, Hangzhou 310018, China

Corresponding author: Qiuzhen Yan (zjhzyqz@gmail.cn)

This work was supported in part by the National Natural Science Foundation of China under Grant 61801431, and in part by the Zhejiang Provincial Natural Science Foundation of China under Grant LY22F030011.

ABSTRACT Pneumatic muscle actuators are widely used in the manufacture of bionic robots and rehabilitation medical equipment. However, due to complicated inherent nonlinearities, time-varying characteristics and uncertainties, it is still a challenge to carry out the accurate dynamic modeling and controller design for PAM systems. To address above issues, we propose an error tracking-based neuro-adaptive iterative learning control scheme to get satisfactory non-uniform angle trajectory tracking performance. First, the error-tracking method is used to overcome the nonzero initial state error in iterative learning controller design for the PAM system. Second, a difference-learning neural network is utilized to compensate for unknown uncertainties in the PAM system dynamics. Moreover, a barrier Lyapunov function is applied to design controller so as to restrict the the difference between system out error and the desired error trajectory within the preset bound during each iteration. And the stability of the closed-loop system is proven theoretically by using Lyapunov synthesis. Finally, simulation results demonstrate the effectiveness of the proposed control scheme.

INDEX TERMS Pneumatic artificial muscle systems, iterative learning control, barrier Lyapunov function, error tracking method, neural network control.

I. INTRODUCTION

With the rapid development of robot technology, the engineering and scientific community are eagerly looking forward to the advent of actuators and electromechanical system with better performance [1]. Pneumatic artificial muscle(PAM) is a kind of soft tubular actuator possessing many advantages, such as rapid response, low cost, high power weight ratio, etc [2], [3], [4]. These above-mentioned merits propels the increasing attention and wide application of PAM actuators in the field of bionic robots, exoskeleton and rehabilitation robots. Nevertheless, there exist complicated inherent characteristics in PAM systems, inclusive of high nonlinearities, complex hysteresis, and time-varying characteristics, such that the controller design of PAM systems is challenging. The past decades have witnessed the hard exploration in the study of controller design for PAM systems, which yields some meaningful results based on sliding mode control technique [5], adaptive control theory [6], [7], predictive control method [8], fuzzy control theory [9], ADRC theory [10], [11], etc. In many occasions, PAM-actuated rehabilitation devices are applied for performing repeated tasks, e.g., the lower limb assistance devices used to assist walking and help rehabilitation training. As such, iterative learning control (ILC) technique may be adopted for obtaining excellent tracking performance. ILC is a distinctive control strategy good at dealing with repeated tracking control or periodic disturbance rejection according to iterative learning strategy for nonlinear systems [12], [13], [14], [15]. While ILC systems operate, the iteration-independent uncertainties in ILC systems may be estimated by using system errors, cycle by cycle. Through these self-tuning processes, ILC systems

The associate editor coordinating the review of this manuscript and approving it for publication was Min Wang.

can improve the control performances gradually, even with little knowledge of the system model.

Two aspects of ILC algorithm designs for PAM systems will be considered in this work. The first aspect with ILC on PAM systems is about the non-uniform trajectory tracking for nonlinear systems with nonzero initial errors. In most traditional ILC results, the reference trajectory must be iteration-invariant. Nevertheless, in some cases, we possibly encounter the cases that the reference trajectory in one iteration cycle is different from the reference trajectory in another iteration cycle. In the context of PAM systems, the control task probably changes in iteration domain, which means the reference trajectory should be adjusted to meet the demand. Only a few ILC literature results have ever reported ILC scheme in the case of tracking non-uniform trajectory during different iterations [16], [17], [18]. Specifically, in [16], an ILC design based on contraction mapping principle is developed for the situation where the reference signal slowly varies between two adjacent iterations. In [17], the non-uniform trajectory tracking design based on Lyapunov approach is studied, where the reference trajectories in one iteration is totally different from that in another iteration. In [18], the non-repetitive trajectory tracking ILC scheme is developed for nonparametric uncertain systems. In [16] and [17], the initial system error in each iteration is assumed to be zero. Due to limitations of physical resetting, it is difficult to let the initial error be zero in many practical situations. Hence, it is of significance to develop adaptive ILC schemes suitable to nonzero initial errors, which is a fundamental problem of ILC and is usually called the initial position problem of ILC in the field of ILC. To broaden the application scope of ILC technology, several solutions have been put forward, such as time-varying boundary layer [19], initial rectification action [18], [20] and error tracking method [21]. But overall, the number of solutions is still very limited. Therefore, the initial position problem of ILC deserves further study. To the best of our knowledge, though there are some existing results involved with ILC design for PAM systems [22], the non-uniform trajectory tracking ILC design for PAM systems with nonzero initial error has not addressed yet.

The second problem is about system constraints of PAM systems. In many practical systems, there exist various constraints. If the system output or system state violates a certain constraint, it may result in performance degradation and system insecurity. Up to now, the typical constraint control design includes model predictive control [24], set invariance notions [23], reference governor [25] and barrier Lyapunov function [26], [27], [28]. The adaptive control for PAM systems with system constraint is investigated in [6]. To the best of our knowledge, the existing result on adaptive ILC for PAM systems with system constraints is very few [29]. In [29], an adaptive ILC law is developed for PAM systems whose filtering error are constrained during system operations. How to address the issue of non-uniform trajectory tracking and output constraint in adaptive ILC design for PAM systems with nonzero initial errors, is a significant research topic yet to be resolved.

Inspired by the above discussion, to solve the angle non-uniform trajectory tracking problem of PAM systems, we will develop an output-constrained error-tracking adaptive ILC scheme for a PAM-actuated device. Compared with existing results, the main contributions can be summarized as follows:

(1) Non-uniform trajectory tracking of PAM systems has been considered with an error-tracking method adopted for dealing with the problem of nonzero initial error in ILC design.

(2) It is the first time to develop adaptive ILC scheme for PAM systems with output constraint, which is different from the filtering-error constraint strategy given in [29].

(3) By developing a barrier Lyapunov functional, along with the difference-learning neural network, excellent control performance and the boundedness of all signals in the closed-loop system are guaranteed.

The paper is organized as follows. The system model and problem formulation is introduced in Section II. In Section III, a simple example is provided to clearly explain how to use the error-tracking method during ILC system design. The construction of auxiliary curves and the detailed procedure of controller design is given in Section IV. The stability analysis of closed-loop PAM system is provided in Section V. The satisfactory simulation results are shown in Section VI, and the conclusion is drawn in Section VII.

II. PROBLEM FORMULATION

The model a PAM-acutated device [6] is presented in Fig. 1. The control objective is to make the PAM system with complicated inherent dynamic characteristics, uncertainties and disturbance track the given reference trajectories, so as to further complete actuating tasks.

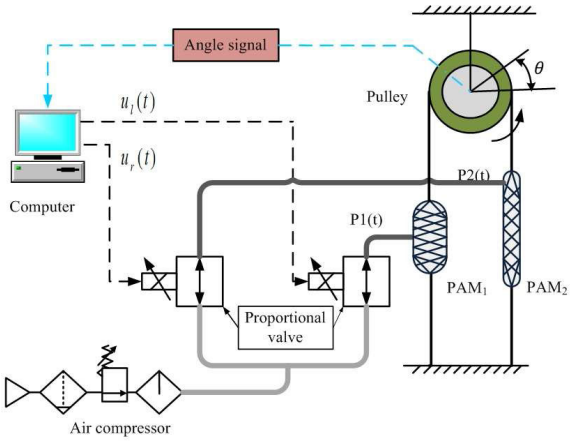

FIGURE 1. Control system structure of the PAM-actuated mechanism.

In this device, there exist two PAM actuators which are parallel to each other. The signal of deflection angle may be collected by the angle sensor and then be transmitted to the computer. The charging or discharging of the two PAM

actuators can be realized by opening and closing the pressure proportional valves. The input control voltages of pressure proportional valves, $u_l(t)$ and $u_r(t)$, are determined by the following equations.

$$\begin{cases} u_l(t) = u_o + \delta_u u(t), \\ u_r(t) = u_o - \delta_u u(t), \end{cases} \tag{1}$$

in which u_o presents the preloaded voltage, $u(t)$ is the control input and δ_u denotes the coefficient of voltage distribution. Here, $t \in [0, T]$, T denotes the operation time interval during each iteration. P_1 and P_2 are the internal pressures of two PAM actuators, which can be calculated by

$$\begin{cases} P_1(t) = P_0 + \Delta P(t) = \delta_0 u_l(t), \\ P_2(t) = P_0 - \Delta P(t) = \delta_0 u_r(t). \end{cases} \tag{2}$$

In (2), P_0 presents the preloaded internal pressure, $\Delta P(t)$ is the variation of pressure, and δ_0 denotes the proportional coefficient of the control voltage and output pressure. $F_1(t)$ and $F_2(t)$ are the Pulling forces generated by PAM actuators, which may be determined by

$$\begin{cases} F_1(t) = P_1(t)(\lambda_1 \epsilon_1^2(t) + \lambda_2 \epsilon_1(t) + \lambda_3) + \lambda_4, \\ F_2(t) = P_2(t)(\lambda_1 \epsilon_2^2(t) + \lambda_2 \epsilon_1(t) + \lambda_3) + \lambda_4, \end{cases} \tag{3}$$

where $\lambda_1 - \lambda_4$ are four parameters, $\epsilon_1(t) = \epsilon_0 + r l_0^{-1}\theta(t)$, and $\epsilon_2(t) = \epsilon_0 - r l_0^{-1}\theta(t)$. Here, $\theta(t)$ is the deflection angle, ϵ_0 is the initial shrinking rate, and l_0 represents the initial length of PAM actuators. By letting J_p represent the moment of inertia, b_υ denote the damping coefficient and r be the radius of pulley, we can deduce the driving moment of this device as

$$T_p(t) = J_p \ddot{\theta}(t) + b_\upsilon \dot{\theta}(t) = F_1(t) r - F_2(t) r + d_\upsilon, \tag{4}$$

in which d_υ is the unknown external disturbances. From (1)- (4), we obtain

$$\begin{aligned} \ddot{\theta}(t) = & -J_p^{-1} b_v \dot{\theta}(t) + 2J k_0 u_o r^2 (2\lambda_1 \epsilon_0 + \lambda_2) l_0^{-1} \theta(t) \\ & + 2J_p^{-1} k_0 \lambda_u r [\lambda_1 \epsilon_0^2 + \lambda_2 \epsilon_0 + \lambda_3 + 2\lambda_2 \epsilon_0 \\ & + \lambda_1 (r\theta(t) l_0^{-1})^2] u(t) + d_s \end{aligned} \tag{5}$$

where $d_s = J_p^{-1} d_\upsilon$. Let $x_1(t)$ and $x_2(t)$ denote $\theta(t)$ and $\dot{\theta}(t)$, respectively. From (5), we can get the state-space model of the device at the kth iteration cycle as

$$\begin{cases} \dot{x}_{1,k}(t) = x_{2,k}(t), \\ \dot{x}_{2,k}(t) = u_o \xi_1 x_{1,k}(t) + \xi_2 x_{2,k}(t) + [g_1 + g_2 x_{1,k}^2] u_k(t) \\ \quad + d_{s,k}, \end{cases} \tag{6}$$

where $\xi_1 = 2J^{-1} k_0 r^2 (2\lambda_1 \epsilon_0 + \lambda_2) l_0^{-1}$, $\xi_2 = -J^{-1} b_v$ and $g_1 = 2J^{-1} k_0 \lambda_u r (\lambda_1 \epsilon_0^2 + \lambda_2 \epsilon_0 + \lambda_3)$, $g_2 = 2J^{-1} k_0 \lambda_u r \lambda_1 (r l_0^{-1})^2$.

For simplicity, the arguments of functions in the article are often omitted when no confusion occurs.

III. A SIMPLE EXAMPLE ON ERROR TRACKING METHOD

To clearly explain the concept of initial position problem of ILC and how to solve this problem by using error-tracking method [20], let us consider a simple system as follows:

$$\dot{\chi}_k(t) = \vartheta(t) \sin(\chi_k) + u_k(t), \tag{7}$$

where k denotes iteration index, $t \in [0, 5]$, $\chi_k(t) \in \mathbb{R}$, $\vartheta(t)$ is an unknown parameter. Assume $\vartheta(t)$ is time-varying but iteration-independent, i.e., $\vartheta(t) = 2\mathrm{e}^{0.01\,t} + \sin(0.2\pi t)$. The control objective is to make $\chi_k(t)$ converge to zero as k increases. Because $\vartheta(t)$ is time-varying, we will derive a difference learning law to estimate $\vartheta(t)$.

s1). Design control law and iterative learning laws as

$$u_k = -\iota \chi_k - \vartheta_k \sin(\chi_k), \tag{8}$$

$$\vartheta_k = \vartheta_{k-1} + \chi_k \sin(\chi_k), \tag{9}$$

where $\iota > 0$ is a design parameter. Substituting (8) into (7) leads to

$$\dot{\chi}_k(t) = -\iota \chi_k + \tilde{\vartheta}_k \sin(\chi_k), \tag{10}$$

where $\tilde{\vartheta}_k = \vartheta - \vartheta_k$. Define a Lyapunov functional as

$$L_{\chi,k} = \frac{1}{2}\chi_k^2 + \frac{1}{2}\int_0^t \tilde{\vartheta}_k^2 d\tau. \tag{11}$$

From (11), we obtain

$$L_{\chi,k} - L_{\chi,k-1} = \frac{1}{2}\chi_k^2 - \frac{1}{2}\chi_{k-1}^2 + \frac{1}{2}\int_0^t (\tilde{\vartheta}_k^2 - \tilde{\vartheta}_{k-1}^2) d\tau. \tag{12}$$

By (10), we have

$$\begin{aligned} \frac{1}{2}\chi_k^2 &= \frac{1}{2}\chi_k^2(0) + \int_0^t \chi_k \dot{\chi}_k d\tau \\ &= \frac{1}{2}\chi_k^2(0) - \iota \int_0^t \chi_k^2 d\tau + \int_0^t \chi \tilde{\vartheta}_k \sin(\chi_k) d\tau. \end{aligned} \tag{13}$$

Substituting (13) into (12) yields

$$\begin{aligned} L_{\chi,k} - L_{\chi,k-1} \le & \frac{1}{2}\chi_k^2(0) + \int_0^t \chi \tilde{\vartheta}_k \sin(\chi_k) d\tau - \frac{1}{2}\chi_{k-1}^2 \\ & + \frac{1}{2}\int_0^t (\tilde{\vartheta}_k^2 - \tilde{\vartheta}_{k-1}^2) d\tau. \end{aligned} \tag{14}$$

It follows from (9) that

$$\begin{aligned} & \chi \tilde{\vartheta}_k \sin(\chi_k) + \frac{1}{2}(\tilde{\vartheta}_k^2 - \tilde{\vartheta}_{k-1}^2) \\ & = \chi \tilde{\vartheta}_k \sin(\chi_k) + \frac{1}{2}(2\vartheta - \vartheta_k - \vartheta_{k-1})(\vartheta_{k-1} - \vartheta_{k-1}) \\ & \le \chi \tilde{\vartheta}_k \sin(\chi_k) + \frac{1}{2}(2\vartheta - 2\vartheta_k)(\vartheta_{k-1} - \vartheta_{k-1}) \\ & = 0. \end{aligned} \tag{15}$$

Combining (14) with (15), we get

$$L_{\chi,k} - L_{\chi,k-1} \le \frac{1}{2}\chi_k^2(0) - \frac{1}{2}\chi_{k-1}^2. \tag{16}$$

By recursion method, from (16), we obtain

$$\frac{1}{2}\chi_k^2(t) \le L_{\chi,k}(t) \le L_{\chi,0}(t) + \frac{1}{2}\sum_{i=0}^{k}\chi_i^2(0) - \frac{1}{2}\chi_{k-1}^2(t). \tag{17}$$

$L_{\chi,0}(t)$ can be proved to be bounded. If $\chi_i(0) = 0$ holds, from (17), we can derive the conclusion that $L_{\chi,k}(t) = 0$ and $\chi_k(t) = 0$ for $k \to +\infty$. If the boundedness of $\sum_{i=0}^{k}\chi_i^2(0)$ can not be guaranteed, from (17), we can not derive the conclusion that $L_{\chi,k}(t) = 0$ and $\chi_k(t) = 0$ for $k \to +\infty$.

Remark 1: In practical applications, the initial state of the system is not equal to 0, which means $\chi_i(0)$ is not equal to 0 here. From this, it can be inferred that $\sum_{i=0}^{k}\chi_i^2(0) \to +\infty$ while $k \to +\infty$, which means we can not derive the conclusion that $L_{\chi,k}(t) = 0$ and $\chi_k(t) = 0$ for $k \to +\infty$ from (17). Hence, traditional ILC algorithms are not applicable in many practical applications.

s2) Define

$$\chi_k^*(t) = \chi_k(0)h_\chi(t)\cos(\frac{\pi t}{2t_\delta}), \tag{18}$$

where $0 < t_\delta < 5(e.g.,\ t_\delta = 0.5)$, and

$$h_\chi(t) = \begin{cases} 1, & \text{for } t \le t_\delta, \\ 0, & \text{for } t > t_\delta. \end{cases} \tag{19}$$

Let us define

$$\chi_{z,k}(t) = \chi_k(t) - \chi_k^*(t). \tag{20}$$

According to (7) and (20), we have

$$\dot{\chi}_{z,k}(t) = \vartheta(t)\sin(\chi_k) + u_k(t) - \dot{\chi}_k^*, \tag{21}$$

On the basis of (21), we design the control law and iterative learning law as

$$u_k = -\iota\chi_{z,k} - \vartheta_k\sin(\chi_k), \tag{22}$$

$$\vartheta_k = \vartheta_{k-1} + \chi_{z,k}\sin(\chi_k). \tag{23}$$

Define another Lyapunov functional as

$$L_{z,k} = \frac{1}{2}\chi_{z,k}^2 + \frac{1}{2}\int_0^t \tilde{\vartheta}_k^2 d\tau. \tag{24}$$

Similar to (17), we can obtain

$$L_{z,k}(t) \le L_{z,0}(t) + \frac{1}{2}\sum_{i=0}^{k}\chi_{z,i}^2(0) - \frac{1}{2}\chi_{k-1}^2 \tag{25}$$

It follows from (25) that

$$\frac{1}{2}\chi_{z,k}^2(t) \le L_{z,k}(t) \le L_{z,0}(t) - \frac{1}{2}\chi_{k-1}^2(t) \tag{26}$$

From (26), we can derive the conclusion that $L_{z,k}(t) = 0$ and $\chi_{z,k}(t) = 0$ for $t \in [0, 5]$ and for $k \to +\infty$. Thus, based on the fact that $\chi_{z,k}(t) = \chi_k(t)$ for $t \in [t_\delta, 5]$, $\chi_k(t) = 0$ holds over $t \in [t_\delta, 5]$, while $k \to +\infty$.

According to the above analysis, we can see that the control algorithm (22)-(23) may be used in cases that $\chi_k(0) \ne 0$. That is to say, the design method is effective to solve the initial position problem of ILC.

Remark 2: Because $\chi_{z,i}(0) = 0$ for $i = 0, 1, \cdots, k$, so the term $\frac{1}{2}\sum_{i=0}^{k}\chi_{z,i}^2(0)$ in (25) is equal to zero. By contrast, the term $\frac{1}{2}\sum_{i=0}^{k}\chi_i^2(0)$ in (17) is not equal to zero.

IV. CONTROLLER DESIGN

Let $x_{1,d}$ denote the reference trajectory. By defining $e_{1,k} = x_{1,k} - x_{1,d}$, $e_{2,k} = x_{1,k} - x_{2,d}$ and $x_{2,d} = \dot{x}_{1,d}$, from (6), we have

$$\begin{cases} \dot{e}_{1,k} = e_{2,k}, \\ \dot{e}_{2,k} = u_{o,k}\xi_1 x_{1,k} + \xi_2 x_{2,k} + (g_1 + g_2 x_{1,k}^2)u_k + d_{s,k} \\ \quad -\ddot{x}_{1,d}. \end{cases} \tag{27}$$

Note that in actual situations, the initial system error in each iteration usually satisfies

$$e_{1,k}(0) \ne 0,\ e_{2,k}(0) = 0. \tag{28}$$

A. CONSTRUCTION OF DESIRED ERROR TRAJECTORY

To overcome the obstacle caused by nonzero initial error in the path of of ILC system design, two auxiliary signals $e_{1,k}^*(t)$ and $e_{2,k}^*(t)$ are formed as follows:

When $0 \le t \le t_\delta$,

$$e_{1,k}^*(t) = e_{1,k}(0)\big(\frac{10(t_\delta - t)^3}{t_\delta^3} - \frac{15(t_\delta - t)^4}{t_\delta^4} + \frac{6(t_\delta - t)^5}{t_\delta^5}\big), \tag{29}$$

$$e_{2,k}^*(t) = e_{1,k}(0)\big(-\frac{30(t_\delta - t)^2}{t_\delta^3} + \frac{60(t_\delta - t)^3}{t_\delta^4} - \frac{30(t_\delta - t)^4}{t_\delta^5}\big), \tag{30}$$

when $t_\delta < t \le T$, $e_{1,k}^*(t) = 0$, $e_{2,k}^*(t) = 0$. Here, t_δ is a preset time point between 0 and T.

Let $\varepsilon_{1,k}(t) = e_{1,k}(t) - e_{1,k}^*(t)$ and $\varepsilon_{2,k}(t) = e_{2,k}(t) - e_{2,k}^*(t)$. Through simple calculation, it follows from (29) that $e_{1,k}^*(0) = e_{1,k}(0)$ holds. Meanwhile, when $t = 0$,

$$\frac{-30(t_\delta - t)^2}{t_\delta^3} + \frac{60(t_\delta - t)^3}{t_\delta^4} - \frac{30(t_\delta - t)^4}{t_\delta^5} = 0, \tag{31}$$

from which and (30), it can be inferred that $e_{2,k}^*(0) = 0$ holds.

Based on the fact that $e_{1,k}^*(0) = e_{1,k}(0)$ and $e_{2,k}(0) = e_{2,k}^*(0) = 0$, it is obvious that

$$\varepsilon_{1,k}(0) = 0,\ \varepsilon_{2,k}(0) = 0. \tag{32}$$

B. ERROR-TRACKING CONTROLLER DESIGN

According to (27), we get

$$\begin{cases} \dot{\varepsilon}_{1,k} = \varepsilon_{2,k}, \\ \dot{\varepsilon}_{2,k} = u_{o,k}\xi_1 x_{1,k} + \xi_2 x_{2,k} + (g_1 + g_2 x_{1,k}^2)u_k \\ \quad +d_{s,k} - \ddot{x}_{1,d} - \dot{e}_{2,k}^*. \end{cases} \tag{33}$$

Define $s_{\varepsilon,k} = c\varepsilon_{1,k} + \varepsilon_{2,k}$ with $c > 0$. From (33), the derivative of $s_{\varepsilon,k}$ may be calculated by

$$\dot{s}_{\varepsilon,k} = c\varepsilon_{2,k} + u_{o,k}\xi_1 x_{1,k} + \xi_2 x_{2,k} + (g_1 + g_2 x_{1,k}^2)u_k + d_{s,k} - \ddot{x}_{1,d} - \dot{e}_{2,k}^*. \tag{34}$$

Chose a barrier Lyapunov function as

$$V_k = \frac{\varepsilon_{1,k}^2}{2(b_\varepsilon^2 - \varepsilon_{1,k}^2)} + \frac{1}{2g_1}s_{\varepsilon,k}^2, \tag{35}$$

where $b_\varepsilon > 0$.

Remark 3: On the basis of above conclusions given in (32), we can see that $s_{\varepsilon,k}(0) = 0$ and $V_k(0) = 0$ holds, which is useful to overcome the initial position problem of ILC.

Differentiating V_k yields

$$\begin{aligned}\dot{V}_k &= \frac{b_\varepsilon^2}{(b_\varepsilon^2 - \varepsilon_{1,k}^2)^2}\varepsilon_{1,k}(s_{\varepsilon,k} - c\varepsilon_{1,k}) + s_{\varepsilon,k}\big[g_1^{-1}(c\varepsilon_{2,k} \\ &\quad + u_{o,k}\xi_1 x_{1,k} + \xi_2 x_{2,k} + d_{s,k} - \ddot{x}_{1,d} - \dot{e}_{2,k}^*) \\ &\quad + u_k + g_1^{-1}g_2 x_{1,k}^2 u_k\big] \\ &\le \frac{b_\varepsilon^2 \varepsilon_{1,k} s_{\varepsilon,k}}{(b_\varepsilon^2 - \varepsilon_{1,k}^2)^2} + s_{\varepsilon,k}\big[g_1^{-1}(c\varepsilon_{2,k} + u_{o,k}\xi_1 x_{1,k} + \xi_2 x_{2,k} \\ &\quad + d_{s,k} - \ddot{x}_{1,d} - \dot{e}_{2,k}^*) + u_k + g_1^{-1}g_2 x_{1,k}^2 u_k\big]. \end{aligned} \tag{36}$$

Then, a radial basis function (RBF) neural network is adopted for constructing the following approximator

$$\begin{aligned} &g_1^{-1}(c\varepsilon_{2,k} + u_{o,k}\xi_1 x_{1,k} + \xi_2 x_{2,k} + d_{s,k} - \ddot{x}_{1,d} - \dot{e}_{2,k}^*) \\ &\quad = \boldsymbol{\eta}^{*T}(t)\boldsymbol{\psi}(\boldsymbol{X}) + \epsilon(\boldsymbol{X}), \end{aligned} \tag{37}$$

in which $\boldsymbol{\eta}^*(t)$ represents the optimal weight of neural network and $\boldsymbol{\psi}(\boldsymbol{X}) = [\psi_{1,k}, \psi_{2,k}, \cdots, \psi_{m,k}]^T$, where

$$\psi_{j,k} = \mathrm{e}^{-\frac{\|\boldsymbol{X} - \boldsymbol{c}_j\|^2}{2b_j^2}}, \quad j = 1, 2, \cdots, m, \tag{38}$$

$\boldsymbol{X} = [x_{1,k}, x_{2,k}, x_{1,d}, x_{2,d}, \dot{x}_{2,d}]^T$, $\boldsymbol{c}_j$ and b_j represent the center vector and the width of the hidden layer, respectively. $\epsilon(\boldsymbol{X})$ is the approximation error. There exists an unknown constant ϵ_N such that $|\epsilon(\boldsymbol{X})| \le \epsilon_N$.

Denote $\boldsymbol{\psi}(\boldsymbol{X}_k)$ briefly by $\boldsymbol{\psi}_k$. Combining (36) with (37) yields

$$\begin{aligned}\dot{V}_k &= \frac{b_\varepsilon^2 \varepsilon_{1,k} s_{\varepsilon,k}}{(b_\varepsilon^2 - \varepsilon_{1,k}^2)^2} + s_{\varepsilon,k}[\boldsymbol{\eta}^{*T}(t)\boldsymbol{\psi}_k + \epsilon(\boldsymbol{x}_k) + u_k \\ &\quad + g_1^{-1}g_2 x_{1,k}^2 u_k] \end{aligned} \tag{39}$$

Based on (39), the control law and iterative learning laws are designed as follows:

$$u_k = u_{i,k} + u_{r,k}, \tag{40}$$

$$u_{i,k} = -\frac{b_\varepsilon^2 \varepsilon_{1,k}}{(b_\varepsilon^2 - \varepsilon_{1,k}^2)^2} - \lambda_s s_{\varepsilon,k} - \boldsymbol{\eta}_k^T \boldsymbol{\psi}_k, \tag{41}$$

$$\begin{aligned} u_{r,k} &= -\varpi_k x_{1,k}^2 u_{i,k} \tanh(s_{\varepsilon,k}\varpi_k x_{1,k}^2 u_{i,k}\upsilon) \\ &\quad - \epsilon_{N,k} \tanh(s_{\varepsilon,k}\epsilon_{N,k}\upsilon), \end{aligned} \tag{42}$$

$$\boldsymbol{\eta_k} = \mathrm{sat}(\boldsymbol{\eta}_{k-1}) + \gamma_1 s_{\varepsilon,k}\boldsymbol{\psi}_k, \boldsymbol{\eta_{-1}} = 0, \tag{43}$$

$$\varpi_k = \mathrm{sat}(\varpi_{k-1}) + \gamma_2 s_{\varepsilon,k} x_{1,k}^2 u_{i,k}, \varpi_{-1} = 0, \tag{44}$$

$$\epsilon_{N,k} = \mathrm{sat}(\epsilon_{N,k-1}) + \gamma_3 |s_{\varepsilon,k}|, \epsilon_{N,-1} = 0, \tag{45}$$

where $\lambda_s > 0$, $\upsilon = \mu(k+1)(k+2)$, $\mu > 0$, $\gamma_1 > 0$, $\gamma_2 > 0$, $\gamma_3 > 0$, ϖ_k is the estimation of $\varpi := g_1^{-1}g_2$, and $\epsilon_{N,k}$ is the estimation of ϵ_N. Here, sat$(\cdot)$ is is an saturation operator: For $\beta \in \mathbb{R}$,

$$\mathrm{sat}(\beta) := \mathrm{sign}(\beta)\min(\bar{\beta}, |\beta|), \tag{46}$$

in which $\bar{\beta}$ represents the upper bound of $|\beta|$ and sign$(\cdot)$ is an operator of signum function; for an n-dimensional vector $\boldsymbol{\beta} = [\beta_1, \beta_2, \cdots, \beta_n]^T$, sat$(\boldsymbol{\beta}) := [\mathrm{sat}(\beta_1), \mathrm{sat}(\beta_2), \cdots, \mathrm{sat}(\beta_n)]^T$.

V. CONVERGENCE ANALYSIS

Theorem 1: Consider the closed-loop PAM system consisting of (6) and (40)-(45). The tracking performance and system stability can be concluded as follows:

(t1) $|\varepsilon_{1,k}(t)| < b_\varepsilon$ is guaranteed for $t \in [0, T]$, which means $|x_{1,k}| < b_\varepsilon + |x_{1,d}|$ holds for $t \in [t_\delta, T]$.

(t2) Both $e_{1,k}(t) = 0$ and $e_{2,k}(t) = 0$ hold for $t \in [t_\delta, T]$ as the iteration number increases.

(t3) All internal signals in the closed-loop system are guaranteed to be bounded $\forall t \in [0, T]$ and $\forall k > 0$.

Proof: (t1) First, in order to derive the constraint property of PAM system, let us verify the boundedness of the time derivative of barrier Lyapunov functional L_k, which is defined as follows:

$$\begin{aligned} L_k &= V_k + \frac{1}{2\gamma_1}\int_0^t \tilde{\boldsymbol{\eta}}_k^T \tilde{\boldsymbol{\eta}}_k d\tau + \frac{1}{2\gamma_2}\int_0^t \tilde{\varpi}_k^2 d\tau \\ &\quad + \frac{1}{2\gamma_3}\int_0^t \tilde{\epsilon}_{N,k}^2 d\tau, \end{aligned} \tag{47}$$

where $\tilde{\boldsymbol{\eta}}_k = \boldsymbol{\eta} - \tilde{\boldsymbol{\eta}}_k$. Note $L_k(0)$, the initial value of $L_k(t)$, is bounded. In the next part, we will verify that $\dot{L}_k(t) < +\infty$ is guaranteed for $t \in [0, T]$, so as to derive that $L_k(t) < +\infty$ and $|\varepsilon_{1,k}(t)| < b_\varepsilon$ hold for $t \in [0, T]$.

Substituting (40) and (41) into (39) leads to

$$\begin{aligned}\dot{V}_k &\le -\lambda_s s_{\varepsilon,k}^2 + s_{\varepsilon,k}\tilde{\boldsymbol{\eta}}_k^T\boldsymbol{\psi}_k + |s_{\varepsilon,k}|\epsilon_N - |s_{\varepsilon,k}|\epsilon_{N,k} \\ &\quad + |s_{\varepsilon,k}|\epsilon_{N,k} + s_{\varepsilon,k}\varpi x_{1,k}^2 u_{i,k} - s_{\varepsilon,k}\varpi_k x_{1,k}^2 u_{i,k} \\ &\quad + s_{\varepsilon,k}\varpi_k x_{1,k}^2 u_{i,k} + (1 + g_1^{-1}g_2 x_{1,k}^2)u_{2,k}]. \end{aligned} \tag{48}$$

Invoking (42) and (48), we have

$$\begin{aligned}\dot{V}_k &\le -\lambda_s s_{\varepsilon,k}^2 + s_{\varepsilon,k}\tilde{\boldsymbol{\eta}}_k^T\boldsymbol{\psi}_k + |s_{\varepsilon,k}|\tilde{\epsilon}_{N,k} + s_{\varepsilon,k}\tilde{\varpi}_k x_{1,k}^2 u_{i,k} \\ &\quad + |s_{\varepsilon,k}|\epsilon_{N,k} + s_{\varepsilon,k}\varpi_k x_{1,k}^2 u_{i,k} + (1 + g_1^{-1}g_2 x_{1,k}^2) \\ &\quad \times \big[- \varpi_k x_{1,k}^2 u_{i,k} \tanh(s_{\varepsilon,k}\varpi_k x_{1,k}^2 u_{i,k}\upsilon) - \epsilon_{N,k} \\ &\quad \times \tanh(s_{\varepsilon,k}\epsilon_{N,k}\upsilon)\big]. \end{aligned} \tag{49}$$

where $\tilde{\epsilon}_{N,k} = \epsilon_N - \epsilon_{N,k}$, $\tilde{\varpi}_k = \varpi - \varpi_k$. For $\sigma \in R$, $\omega > 0$, the inequality

$$|\sigma| - \sigma\tanh(\frac{\sigma}{\omega}) \le 0.2785\omega \tag{50}$$

holds. By this property, we obtain

$$\begin{aligned} & s_{\varepsilon,k}\varpi_k x_{1,k}^2 u_{i,k} - s_{\varepsilon,k}(1+g_1^{-1}g_2 x_{1,k}^2)\varpi_k x_{1,k}^2 u_{i,k} \\ & \quad \times \tanh(s_{\varepsilon,k}\varpi_k x_{1,k}^2 u_{i,k}\upsilon) \\ & \le s_{\varepsilon,k}\varpi_k x_{1,k}^2 u_{i,k} - \varpi_k x_{1,k}^2 u_{i,k}\tanh(s_{\varepsilon,k}\varpi_k x_{1,k}^2 u_{i,k}\upsilon) \\ & \le \frac{0.2785}{\mu(k+1)(k+2)} \end{aligned} \tag{51}$$

and

$$\begin{aligned} & |s_{\varepsilon,k}|\epsilon_{N,k} - s_{\varepsilon,k}(1+g_1^{-1}g_2 x_{1,k}^2)\epsilon_{N,k}\tanh(s_{\varepsilon,k}\epsilon_{N,k}\upsilon) \\ & \le |s_{\varepsilon,k}|\epsilon_{N,k} - s_{\varepsilon,k}\epsilon_{N,k}\tanh(s_{\varepsilon,k}\epsilon_{N,k}\upsilon) \\ & \le \frac{0.2785}{\mu(k+1)(k+2)}. \end{aligned} \tag{52}$$

It follows from (49), (51) and (52) that

$$\dot{V}_k \le -\lambda_s s_{\varepsilon,k}^2 + s_{\varepsilon,k}\tilde{\boldsymbol{\eta}}_k^T\boldsymbol{\psi}_k + |s_{\varepsilon,k}|\tilde{\epsilon}_{N,k} + s_{\varepsilon,k}\tilde{\varpi}_k x_{1,k}^2 u_{i,k}. \tag{53}$$

With the help of (53), we get

$$\begin{aligned} \dot{L}_k \le & -\lambda_s s_{\varepsilon,k}^2 + s_{\varepsilon,k}\tilde{\boldsymbol{\eta}}_k^T\boldsymbol{\psi}_k + |s_{\varepsilon,k}|\tilde{\epsilon}_{N,k} \\ & + s_{\varepsilon,k}\tilde{\varpi}_k x_{1,k}^2 u_{i,k} + \frac{0.557}{\mu(k+1)(k+2)} \\ & + \frac{1}{2\gamma_1}\tilde{\boldsymbol{\eta}}_k^T\tilde{\boldsymbol{\eta}}_k + \frac{1}{2\gamma_2}\tilde{\varpi}_k^2 + \frac{1}{2\gamma_3}\tilde{\epsilon}_{N,k}^2. \end{aligned} \tag{54}$$

Invoking (43), (44) and (45), we can deduce the following three inequalities:

$$\begin{aligned} & s_{\varepsilon,k}\tilde{\boldsymbol{\eta}}_k^T\boldsymbol{\psi}_k + \frac{1}{2\gamma_1}\tilde{\boldsymbol{\eta}}_k^T\tilde{\boldsymbol{\eta}}_k \\ & = \frac{1}{2\gamma_1}(\boldsymbol{\eta}^* - \boldsymbol{\eta}_k)^T(2\boldsymbol{\eta}_k - 2\mathrm{sat}(\boldsymbol{\eta}_{k-1}) + \boldsymbol{\eta}^* - \boldsymbol{\eta}_k) \\ & = \frac{1}{2\gamma_1}[-\boldsymbol{\eta}_k^T\boldsymbol{\eta}_k + \boldsymbol{\eta}^{*T}\boldsymbol{\eta}^* - 2\boldsymbol{\eta}^{*T}\mathrm{sat}(\boldsymbol{\eta}_{k-1}) + 2\boldsymbol{\eta}_k^T\mathrm{sat}(\boldsymbol{\eta}_{k-1})] \\ & = -\frac{1}{2\gamma_1}[\boldsymbol{\eta}_k - \mathrm{sat}(\boldsymbol{\eta}_{k-1})]^T[\boldsymbol{\eta}_k - \mathrm{sat}(\boldsymbol{\eta}_{k-1})] \\ & \quad + \frac{1}{2\gamma_1}[\mathrm{sat}(\boldsymbol{\eta}_{k-1}^T)\mathrm{sat}(\boldsymbol{\eta}_{k-1}) + \boldsymbol{\eta}^{*T}\boldsymbol{\eta}^* - 2\boldsymbol{\eta}^T\mathrm{sat}(\boldsymbol{\eta}_{k-1})] \\ & \le \frac{1}{2\gamma_1}[\mathrm{sat}(\boldsymbol{\eta}_{k-1}^T)\mathrm{sat}(\boldsymbol{\eta}_{k-1}) + \boldsymbol{\eta}^{*T}\boldsymbol{\eta}^* - 2\boldsymbol{\eta}^T\mathrm{sat}(\boldsymbol{\eta}_{k-1})], \end{aligned} \tag{55}$$

$$\begin{aligned} & s_{\varepsilon,k}\tilde{\varpi}_k x_{1,k}^2 u_{i,k} + \frac{1}{2\gamma_2}\tilde{\varpi}_k^2 \\ & = \frac{1}{2\gamma_2}[-\varpi_k^2 + \varpi^2 - 2\varpi\,\mathrm{sat}(\varpi_{k-1}) + 2\varpi_k\mathrm{sat}(\varpi_{k-1})] \\ & = \frac{1}{2\gamma_2}[\mathrm{sat}(\varpi_{k-1})\mathrm{sat}(\varpi_{k-1}) + \varpi^2 - 2\varpi\,\mathrm{sat}(\varpi_{k-1})] \\ & \quad - \frac{1}{2\gamma_2}[\varpi_k - \mathrm{sat}(\varpi_{k-1})]^2 \\ & \le \frac{1}{2\gamma_2}[\mathrm{sat}(\varpi_{k-1})\mathrm{sat}(\varpi_{k-1}) + \varpi^2 - 2\varpi\,\mathrm{sat}(\varpi_{k-1})], \end{aligned} \tag{56}$$

and

$$\begin{aligned} & |s_{\varepsilon,k}|\tilde{\epsilon}_{N,k} + \frac{1}{2\gamma_3}\tilde{\epsilon}_{N,k}^2 \\ & = \frac{1}{2\gamma_3}[-\epsilon_{N,k}^2 + \epsilon_N^2 - 2\epsilon\,\mathrm{sat}(\epsilon_{N,k-1}) + 2\epsilon_{N,k}\mathrm{sat}(\epsilon_{N,k-1})] \\ & = \frac{1}{2\gamma_3}[\mathrm{sat}(\epsilon_{N,k-1})\mathrm{sat}(\epsilon_{N,k-1}) + \epsilon_N^2 - 2\epsilon\,\mathrm{sat}(\epsilon_{N,k-1})] \\ & \quad - \frac{1}{2\gamma_3}[\epsilon_{N,k} - \mathrm{sat}(\epsilon_{N,k-1})]^2 \\ & \le \frac{1}{2\gamma_3}[\mathrm{sat}(\epsilon_{N,k-1})\mathrm{sat}(\epsilon_{N,k-1}) + \epsilon_N^2 - 2\epsilon_N\,\mathrm{sat}(\epsilon_{N,k-1})]. \end{aligned} \tag{57}$$

By the property of saturation, we can see that the right values of the three above inequalities are bounded. Therefore, from (54)-(57), we obtain

$$\dot{L}_k < +\infty, \tag{58}$$

which means

$$V_k < +\infty \tag{59}$$

and

$$\frac{\varepsilon_{1,k}^2}{2(b_\varepsilon^2 - \varepsilon_{1,k}^2)} < +\infty. \tag{60}$$

From (60), we can see that $|\varepsilon_{1,k}| < b_\varepsilon$ holds for $t \in [0, T]$.

Remark 4: Based on the construction of $e_{1,k}^*(t)$, the result that $|\varepsilon_{1,k}| < b_\varepsilon$ holds for $t \in [0, T]$ implies that $|e_{1,k}| < b_\varepsilon$ and $|x_{1,k}| < b_\varepsilon + |x_{1,d}|$ hold for $t \in [t_\delta, T]$.

(t2) Second, we will calculate the difference of Lyapunov functional between two adjacent iterations, so as to analyze the convergence of PAM system.

From (53), we get

$$\begin{aligned} V_k \le & V_k(0) - \int_0^t \lambda_s s_{\varepsilon,k}^2 d\tau + \int_0^t (s_{\varepsilon,k}\tilde{\boldsymbol{\eta}}_k^T\boldsymbol{\psi}_k + s_{\varepsilon,k}\tilde{\varpi}_k \\ & \times x_{1,k}^2 u_{i,k})d\tau + \int_0^t |s_{\varepsilon,k}|\tilde{\epsilon}_{N,k}d\tau. \end{aligned} \tag{61}$$

Substituting (61) into (47), we have

$$\begin{aligned} L_k \le & -\int_0^t \lambda_s s_{\varepsilon,k}^2 d\tau + \int_0^t (s_{\varepsilon,k}\tilde{\boldsymbol{\eta}}_k^T\boldsymbol{\psi}_k + s_{\varepsilon,k}\tilde{\varpi}_k x_{1,k}^2 u_{i,k})d\tau \\ & + \int_0^t |s_{\varepsilon,k}|\tilde{\epsilon}_{N,k}d\tau + \frac{1}{2\gamma_1}\int_0^t \tilde{\boldsymbol{\eta}}_k^T\tilde{\boldsymbol{\eta}}_k d\tau \\ & + \frac{1}{2\gamma_2}\int_0^t \tilde{\varpi}_k^2 d\tau + \frac{1}{2\gamma_3}\int_0^t \tilde{\epsilon}_{N,k}^2 d\tau. \end{aligned} \tag{62}$$

When $k > 0$, invoking (62), we obtain

$$\begin{aligned} & L_k - L_{k-1} \\ & \le -\int_0^t \lambda_s s_{\varepsilon,k}^2 d\tau + \int_0^t (s_{\varepsilon,k}\tilde{\boldsymbol{\eta}}_k^T\boldsymbol{\psi}_k + s_{\varepsilon,k}\tilde{\varpi}_k x_{1,k}^2 u_{i,k})d\tau \\ & \quad + \int_0^t |s_{\varepsilon,k}|\tilde{\epsilon}_{N,k}d\tau + \frac{1}{2\gamma_1}\int_0^t (\tilde{\boldsymbol{\eta}}_k^T\boldsymbol{\psi}_k - \tilde{\boldsymbol{\eta}}_{k-1}^T\boldsymbol{\psi}_{k-1})d\tau \\ & \quad + \frac{1}{2\gamma_2}\int_0^t (\tilde{\varpi}_k^2 - \tilde{\varpi}_{k-1}^2)d\tau + \frac{1}{2\gamma_3}\int_0^t (\tilde{\epsilon}_{N,k}^2 - \tilde{\epsilon}_{N,k-1}^2)d\tau \\ & \quad - V_{k-1} + \frac{0.557}{\mu(k+1)(k+2)}. \end{aligned} \tag{63}$$

By the adaptive learning law (43), we have

$$\begin{aligned}
&\frac{1}{2\gamma_1}(\tilde{\boldsymbol{\eta}}_k^T\tilde{\boldsymbol{\eta}}_k-\tilde{\boldsymbol{\eta}}_{k-1}^T\tilde{\boldsymbol{\eta}}_{k-1})+s_{\varepsilon,k}\tilde{\varpi}_k x_{1,k}^2u_{i,k}\\
&\le\frac{1}{2\gamma_1}[(\boldsymbol{\eta}-\boldsymbol{\eta}_k)^T(\boldsymbol{\eta}-\boldsymbol{\eta}_k)-(\boldsymbol{\eta}-\mathrm{sat}(\boldsymbol{\eta}_{k-1}))^T(\boldsymbol{\eta}-\mathrm{sat}(\boldsymbol{\eta}_{k-1}))]\\
&\quad+s_{\varepsilon,k}\tilde{\boldsymbol{\eta}}_k^T\boldsymbol{\psi}_k\\
&\le\frac{1}{2\gamma_1}(2\boldsymbol{\eta}-\boldsymbol{\eta}_k-\mathrm{sat}(\boldsymbol{\eta}_{k-1}))^T(\mathrm{sat}(\boldsymbol{\eta}_{k-1})-\boldsymbol{\eta}_k)+s_{\varepsilon,k}\tilde{\boldsymbol{\eta}}_k^T\boldsymbol{\psi}_k\\
&\le\frac{1}{\gamma_1}(\boldsymbol{\eta}-\boldsymbol{\eta}_k)^T(\mathrm{sat}(\boldsymbol{\eta}_{k-1})-\boldsymbol{\eta}_k)+\gamma_1 s_{\varepsilon,k}\boldsymbol{\psi}_k)\\
&=0. \qquad (64)
\end{aligned}$$

It follows from (63) and (64) that

$$\begin{aligned}
&L_k-L_{k-1}\\
&\le-\int_0^t\lambda_s s_{\varepsilon,k}^2d\tau+\int_0^t s_{\varepsilon,k}\tilde{\varpi}_k x_{1,k}^2u_{i,k}d\tau+\int_0^t|s_{\varepsilon,k}|\tilde{\epsilon}_{N,k}d\tau\\
&\quad+\frac{1}{2\gamma_2}\int_0^t(\tilde{\varpi}_k^2-\tilde{\varpi}_{k-1}^2)d\tau+\frac{1}{2\gamma_3}\int_0^t(\tilde{\epsilon}_{N,k}^2-\tilde{\epsilon}_{N,k-1}^2)d\tau\\
&\quad-V_{k-1}+\frac{0.557}{\mu(k+1)(k+2)}. \qquad (65)
\end{aligned}$$

Using the learning law (44), we have

$$\begin{aligned}
&\frac{1}{2\gamma_2}(\tilde{\varpi}_k^2-\tilde{\varpi}_{k-1}^2)+s_{\varepsilon,k}\tilde{\varpi}_k x_{1,k}^2u_{i,k}\\
&\le\frac{1}{2\gamma_2}[(\varpi-\varpi_k)^2-(\varpi-\mathrm{sat}(\varpi_{k-1}))^2)]+s_{\varepsilon,k}\tilde{\varpi}_k x_{1,k}^2u_{i,k}\\
&\le\frac{1}{2\gamma_2}(2\varpi-\varpi_k-\mathrm{sat}(\varpi_{k-1}))(\mathrm{sat}(\varpi_{k-1})-\varpi_k)\\
&\quad+s_{\varepsilon,k}\tilde{\varpi}_k x_{1,k}^2u_{i,k}\\
&\le\frac{1}{\gamma_2}(\varpi-\varpi_k)(\mathrm{sat}(\varpi_{k-1})-\varpi_k+\gamma_2 s_{\varepsilon,k}x_{1,k}^2u_{i,k})\\
&=0. \qquad (66)
\end{aligned}$$

Combining (65) with (66), we arrive at

$$\begin{aligned}
&L_k-L_{k-1}\\
&\le-\int_0^t\lambda_s s_{\varepsilon,k}^2d\tau+\int_0^t|s_{\varepsilon,k}|\tilde{\epsilon}_{N,k}d\tau+\frac{1}{2\gamma_3}\int_0^t(\tilde{\epsilon}_{N,k}^2\\
&\quad-\tilde{\epsilon}_{N,k-1}^2)d\tau-V_{k-1}+\frac{0.557}{\mu(k+1)(k+2)}. \qquad (67)
\end{aligned}$$

Similarly, invoking the learning law (45), we get

$$\begin{aligned}
&\frac{1}{2\gamma_3}(\tilde{\epsilon}_{N,k}^2-\tilde{\epsilon}_{N,k-1}^2)+|s_{\varepsilon,k}|\tilde{\epsilon}_{N,k}\\
&\le\frac{1}{2\gamma_3}[(\epsilon_N-\epsilon_{N,k})^2-(\epsilon_N-\mathrm{sat}(\epsilon_{k-1}))^2]+|s_{\varepsilon,k}|\tilde{\epsilon}_k\\
&\le\frac{1}{2\gamma_3}(2\epsilon_N-\epsilon_{N,k}-\mathrm{sat}(\epsilon_{N,k-1}))(\mathrm{sat}(\epsilon_{N,k-1})-\epsilon_{N,k})\\
&\quad+|s_{\varepsilon,k}|\tilde{\epsilon}_k\\
&\le\frac{1}{\gamma_3}(\epsilon_N-\epsilon_{N,k})(\mathrm{sat}(\epsilon_{N,k-1})-\epsilon_{N,k})+\gamma_3|s_{\varepsilon,k}|)\\
&=0. \qquad (68)
\end{aligned}$$

Applying (68) to (67), we can get

$$\begin{aligned}
&L_k-L_{k-1}\\
&\le-\int_0^t\lambda_s s_{\varepsilon,k}^2d\tau-V_{k-1}+\frac{0.557}{\mu(k+1)(k+2)}\\
&\le-V_{k-1}+\frac{0.557}{\mu}(\frac{1}{k+1}-\frac{1}{k+2}). \qquad (69)
\end{aligned}$$

On the basis of recursive operation, from (69), we obtain

$$L_k(t)\le L_0(t)+\frac{0.557}{\mu}-\frac{1}{2g_1}\sum_{j=0}^{k-1}s_{\varepsilon,j}^2(t). \qquad (70)$$

With the help of the continuity of Lyapunov functional, we can see that of $L_0(t)$ is bounded for $t\in[0,T]$. Therefore, $L_0(t)+\frac{0.557}{\mu}$ is also bounded. Then, from (70), we obtain

$$\lim_{k\to+\infty}s_{\varepsilon,k}(t)=0,\ t\in[0,T]. \qquad (71)$$

In light of the fact that $s_{\varepsilon,k}=c\varepsilon_{1,k}+\varepsilon_{2,k}$, it follows from (71) that

$$\lim_{k\to+\infty}\varepsilon_{1,k}(t)=0,\forall t\in[0,T] \qquad (72)$$

and

$$\lim_{k\to+\infty}\varepsilon_{2,k}(t)=0,\forall t\in[0,T], \qquad (73)$$

which is actually equivalent to the conclusion that both $e_{1,k}(t)=0$ and $e_{2,k}(t)=0$ hold for $t\in[t_\delta,T]$, as the iteration number k increases.

(t3) Here, let us analyze the boundedness of closed-loop system signals.

Based on (70), the boudedness of L_k is guaranteed, such that $s_{\varepsilon,k}$ is bounded. On the basis of this and the definition of $s_{\varepsilon,k}$, we can see that $\varepsilon_{1,k}$ and $\varepsilon_{2,k}$ are bounded. Further, $\boldsymbol{x}_k$ and $\boldsymbol{e}_k$ may be verified to be bounded. Applying the above conclusion and the property of saturation functions, we can derive the boundedness of u_k. Then, it is not difficult to derive the boundedness of all other signals in the closed-loop PAM system. ■

In this work, we construct the auxiliary signals $e_{1,k}^*$ and $e_{2,k}^*$ to overcome the obstacle of nonzero initial error in adaptive ILC design. Difference learning approch is used to estimate the ideal weight of RBF neural network. Hyperbolic tangent function is used to design robust feedback term.

Remark 5: In (61), if $V_k(0)\neq 0$, then the following inequality can be derived:

$$L_k(t)\le L_0(t)+\sum_{i=0}^{k}V_i(0)+\frac{0.557}{\mu}-\frac{1}{2g_1}\sum_{j=0}^{k-1}s_{\varepsilon,j}^2(t),$$

from which we can not conclude that $\lim_{k\to+\infty}s_{\varepsilon,k}(t)=0$.

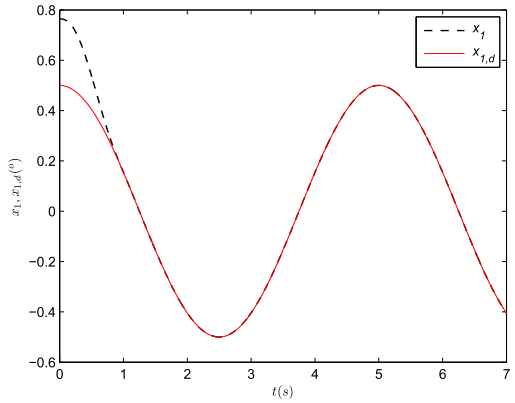

FIGURE 2. x_1 and $x_{1,d}$ during the 29th iteration (barrier ILC).

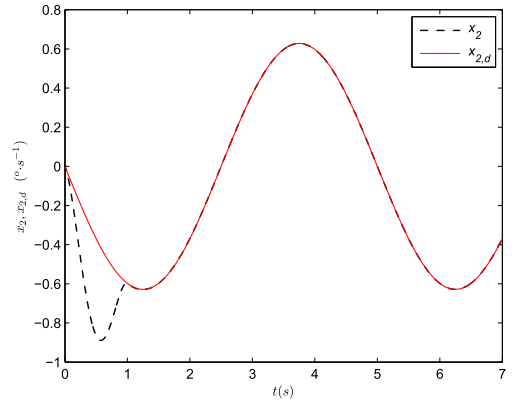

FIGURE 3. x_2 and $x_{2,d}$ during the 29th iteration (barrier ILC).

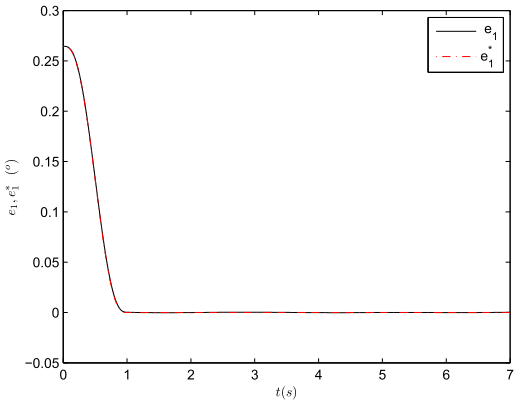

FIGURE 4. The error e_1 and e_1^* during the 29th iteration (barrier ILC).

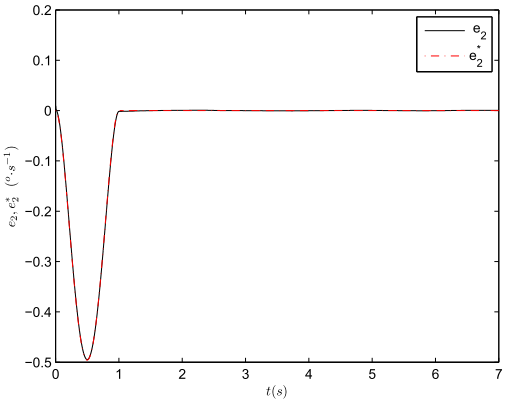

FIGURE 5. The error e_2 and e_2^* during the 29th iteration (barrier ILC).

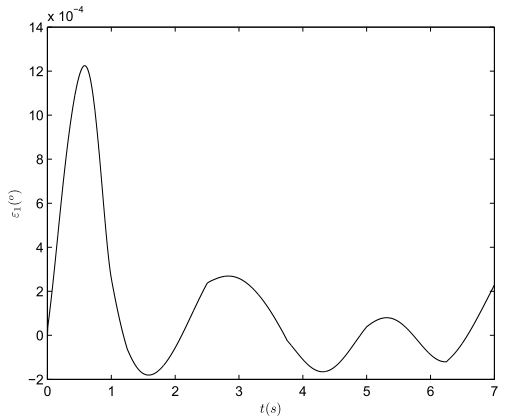

FIGURE 6. ε_1 during the 29th iteration (barrier ILC).

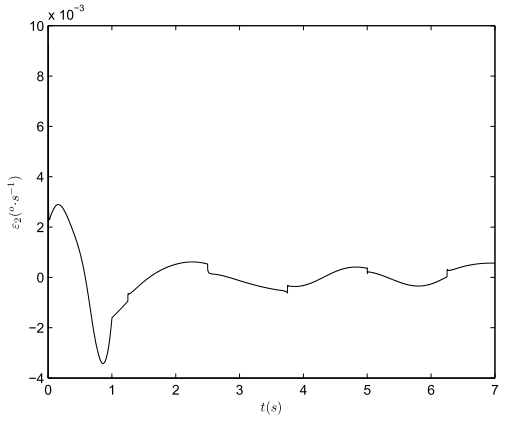

FIGURE 7. ε_2 during the 29th iteration (barrier ILC).

VI. NUMERICAL SIMULATION

To verify the theoretical results, a numerical simulation is performed for the PAM system (6), in which $d_{s,k} = 0.5\sin(x_{1,k})x_{2,k} + 0.1\text{sgn}(x_{1,k}x_{2,k}) + 0.2\text{rand}_1$. The model parameters are set as follows [29]: $\delta_0 = 0.09$, $\lambda_1 = 1$, $\lambda_2 = 1.5$, $\lambda_3 = 4$, $\lambda_4 = 1.8$, $\delta_u = 1$, $\epsilon_0 = 0.5$, $b_v = 2$, $r = 4\text{cm}$, $l_0 = 20\text{cm}$, $u_p = 2.5V$, $J = 10\text{kg}\cdot\text{cm}^2$. The initial state is $x_{1,k}(0) = 0.7 + 0.1\text{rand}_2$, $x_{2,k}(0) = 0$. Here, rand_1 and rand_2 are random numbers between 0 and 1.

The desired trajectory is

$$x_{1,d} = \begin{cases} 0.5\cos(0.4\pi t), & k = 0, 2, 4, 6, \cdots \\ \cos(0.2\pi t), & k = 1, 3, 5, 7, \cdots \end{cases} \tag{74}$$

and

$$x_{2,d} = \begin{cases} -0.2\pi\sin(0.4\pi t), & k = 0, 2, 4, 6, \cdots \\ -0.2\pi\sin(0.2\pi t), & k = 1, 3, 5, 7, \cdots \end{cases} \tag{75}$$

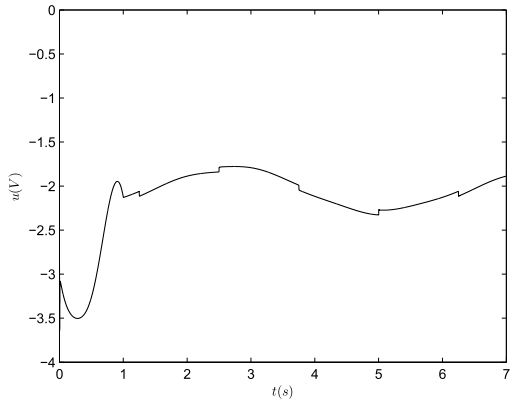

FIGURE 8. Control input during the 29th iteration (barrier ILC).

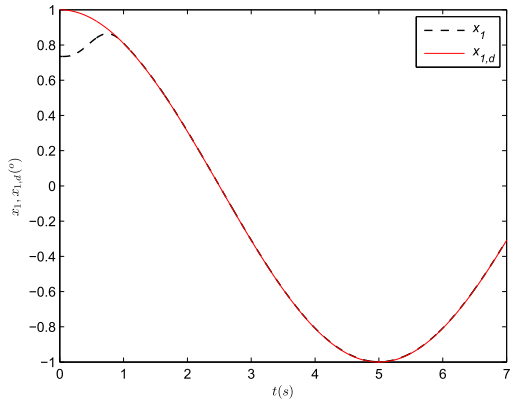

FIGURE 9. x_1 and $x_{1,d}$ during the 30th iteration (barrier ILC).

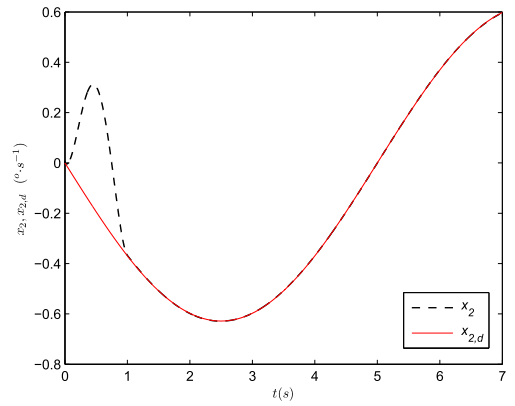

FIGURE 10. x_2 and $x_{2,d}$ during the 30th iteration (barrier ILC).

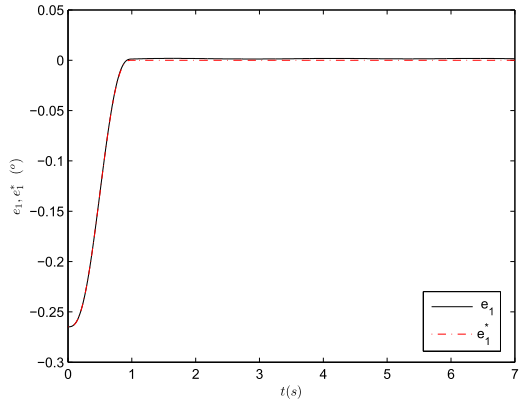

FIGURE 11. The error e_1 and e_1^* during the 30th iteration (barrier ILC).

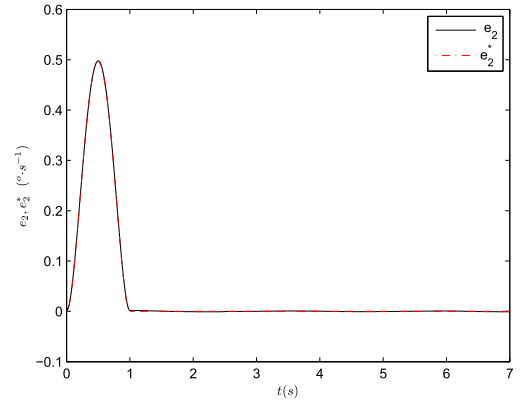

FIGURE 12. The error e_2 and e_2^* during the 30th iteration (barrier ILC).

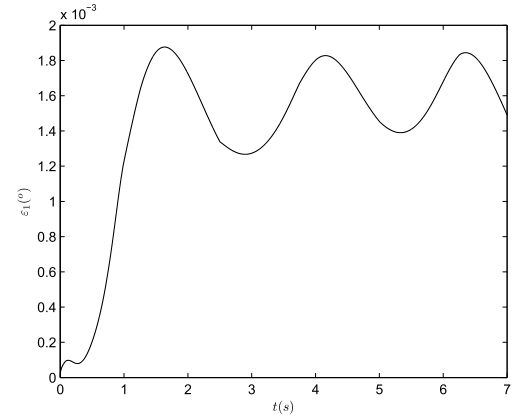

FIGURE 13. ε_1 during the 30th iteration (barrier ILC).

It is obvious that $x_{1,k}(0) \neq x_{1,d}(0)$. The control law and learning laws (40)-(45) is adopted for simulation with $\lambda_s = 5, \mu = 0.1, \gamma_1 = 5, \gamma_2 = 1, \gamma_3 = 0.05, b_\varepsilon = 0.15, t_\delta = 1s, T = 7s$. The number of RBF network neurons in (38) is set to be $m = 5$, with centers c_j, j $= 1, 2, \cdots, m$, evenly spaced on $[-2, 2] \times [-2, 2]$, and the corresponding width $b_j = 3$, j $= 1, 2, \cdots, m$.

The simulation results are shown in Figs. 2-16. The tracking responses of angle position and angular velocity during the 29th iteration are shown in Figs. 2-3 and the tracking responses during the 30th iteration are shown in Figs. 9-10. The angle tracking error and angular velocity tracking error during the 29th iteration are plotted in Figs. 4-5, while the tracking error profiles during the 30th iteration are given in Figs. 11-12. From Figs. 2-5 and Figs. 9-12, we can see that $[x_{1,k}, x_{2,k}]^T$ can precisely track $[x_{1,d}, x_{2,d}]^T$ for $t \in [t_\delta, T]$ during the 29th iteration and the 30th iteration. Meanwhile,

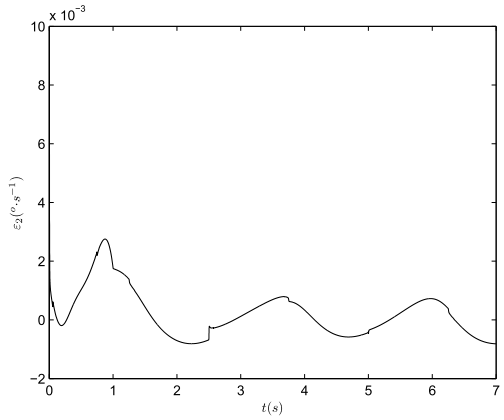

FIGURE 14. ε_2 during the 30th iteration (barrier ILC).

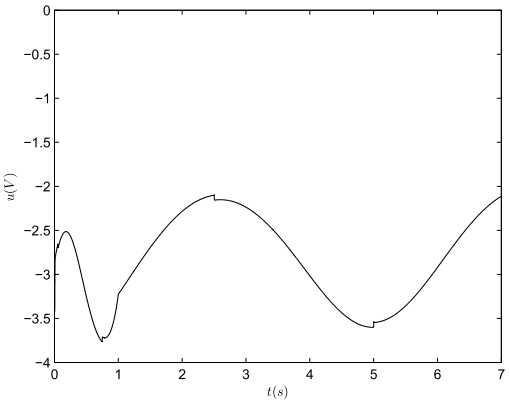

FIGURE 15. Control input during the 30th iteration (barrier ILC).

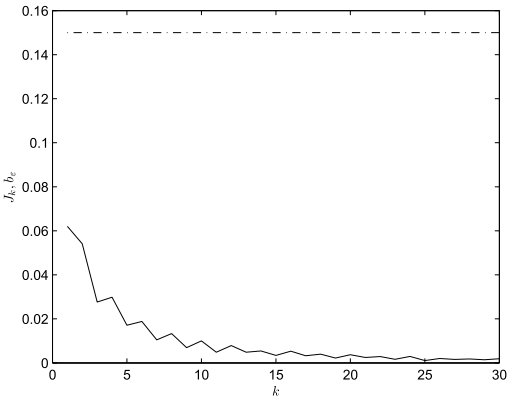

FIGURE 16. History of $\varepsilon_{1,k}$ convergence (barrier ILC, dashed line: b_ε and solid line: J_k).

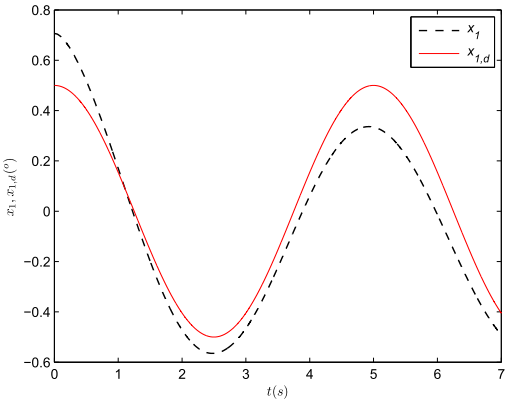

FIGURE 17. x_1 and $x_{1,d}$ during the 29th iteration (PD-type ILC).

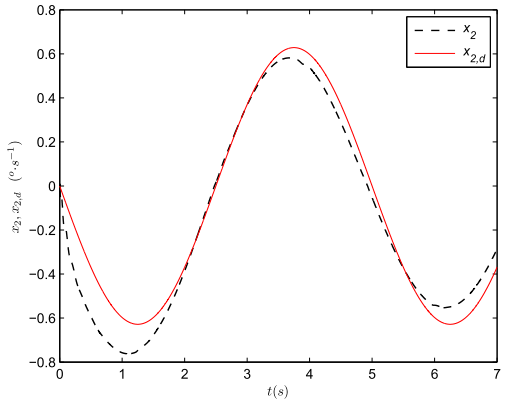

FIGURE 18. x_2 and $x_{2,d}$ during the 29th iteration (PD-type ILC).

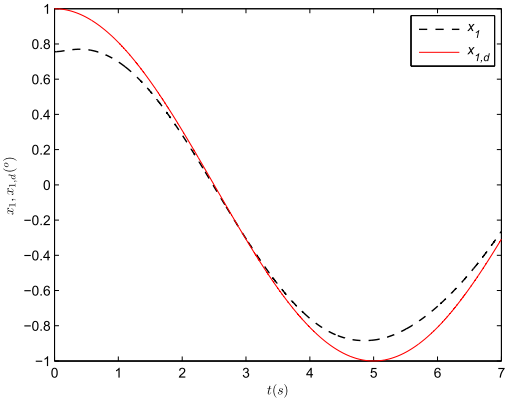

FIGURE 19. x_1 and $x_{1,d}$ during the 30th iteration (PD-type ILC).

it is observed from Figs. 4-7 and Figs. 11-14 that e_1 and e_2 can follow e_1^* and e_2^* over $t \in [0, T]$, respectively. The control input during the 29th iteration and the 30th iteration are shown in Fig. 8 and Fig. 15, respectively. Fig. 16 provides the convergence history of $\varepsilon_{1,k}$, where $J_k \triangleq \max_{t\in[0,T]} |\varepsilon_{1,k}(t)|$. From Fig. 16, we can see that $|\varepsilon_{1,k}(t)| < b_\varepsilon$ holds during system operation.

In the following text, two traditional control algorithms, including robust PD-type ILC algorithm and PID control algorithm, are adopted for comparison as follows.

1). PD-type ILC with forgetting factor [30]:

$$u_{k+1} = \lambda_f u_{k0} + (1 - \lambda_f)u_k + l_p(x_{1,d} - x_{1,k}) + l_d(x_{2,d} - x_{2,k}), \tag{76}$$

in which $0 \leq \lambda_f < 1$ is the forgetting factor, u_{k0} is the preset value of u_k, $l_p > 0$ and $l_d > 0$. In this simulation,

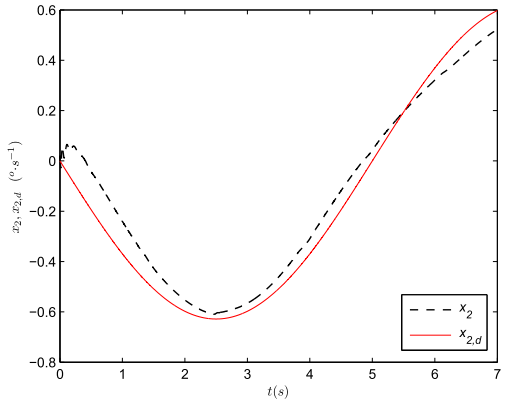

FIGURE 20. x_2 and $x_{2,d}$ during the 30th iteration (PD-type ILC).

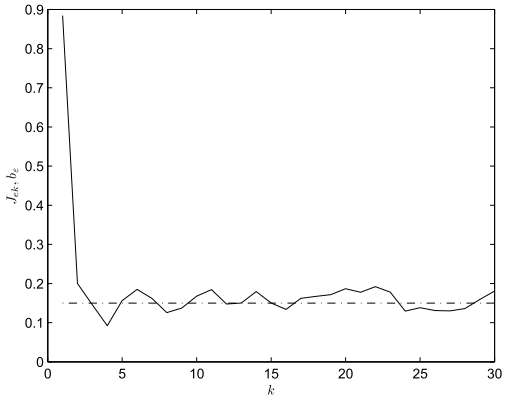

FIGURE 21. History of J_{ek} (PD-type ILC, dashed line: b_e and solid line: J_{ek}).

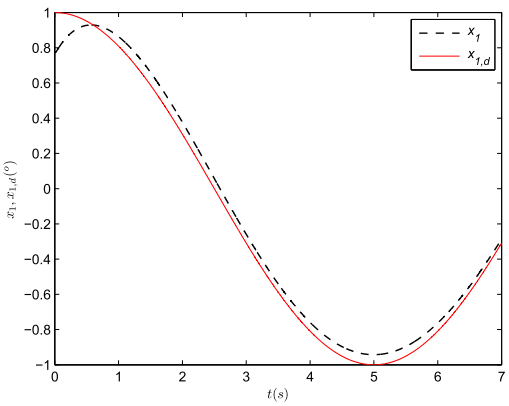

FIGURE 22. x_1 and $x_{1,d}$ (PID control).

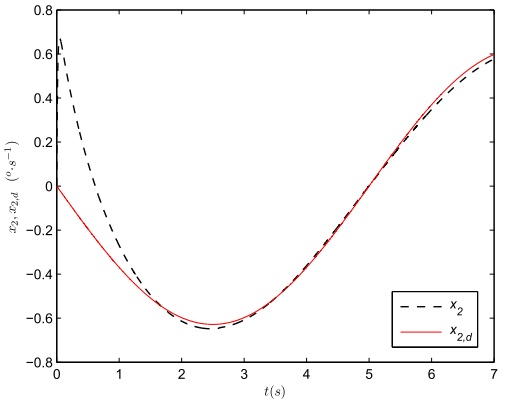

FIGURE 23. x_2 and $x_{2,d}$ (PID control).

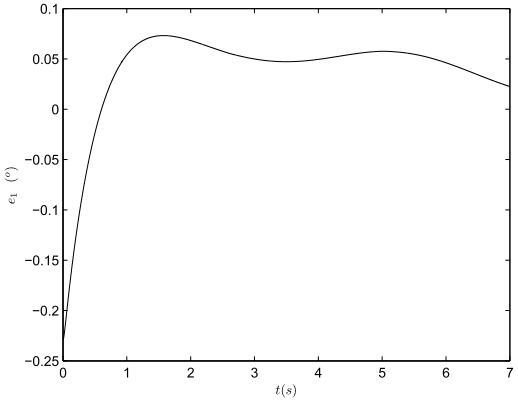

FIGURE 24. The error e_1 (PID control).

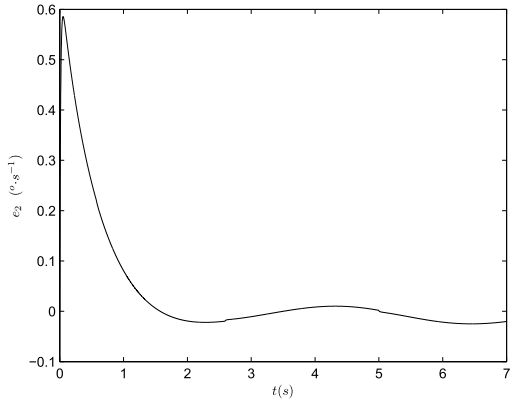

FIGURE 25. The error e_2 (PID control).

they are set as $\lambda_f = 2^{-(k+1)}$, $u_{k0} = 0.5$, $l_p = 5$ and $l_d = 5$. The profiles of angle position tracking and angular velocity tracking during the 29th iteration are shown in Fig. 17 and Fig. 18, respectively. The tracking results during the 30th iteration are shown in Fig. 19 and Fig. 20, respectively. By comparing Figs. 17-18 with Figs. 2-3, as well as Figs. 19-20 with Figs. 9-10, we can be observed that the proposed error-tracking based neuro-adaptive ILC scheme possesses better tracking performance, which indicates that the control algorithm (76) is not suitable for the non-uniform trajectory tracking ILC design for PAM systems with nonzero initial errors. In Fig. 21, J_{ek} denotes $\max_{t\in[t_\delta,T]}|e_{1,k}(t)|$ with $t_\delta = 1$. Comparing Fig. 16 and Fig. 21, we can see the constraint property is guaranteed in the proposed proposed error-tracking based neuro-adaptive ILC, whereas no constraint property is met in PD-type ILC with forgetting factor.

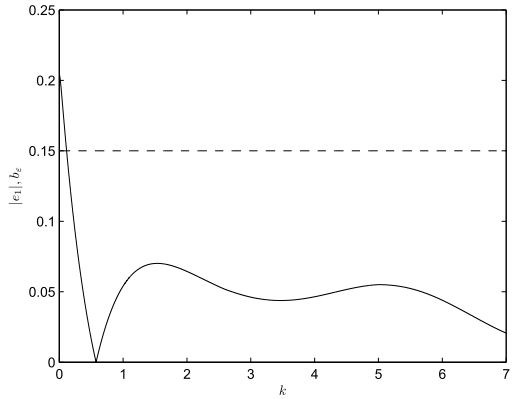

FIGURE 26. The absolute value of e_1 (PID control).

2). PID control:

$$u = \lambda_p(x_{1,d}(t) - x_1(t)) + \lambda_i \int_0^t (x_{1,d}(\tau) - x_1(\tau))d\tau + \lambda_d(\dot{x}_{1,d}(t) - \dot{x}_1(t)), \quad (77)$$

where $x_{1,d} = 0.5\cos(0.4\pi t)$ and the control parameters are chosen as $\lambda_p = 18.2, \lambda_i = 0.5, \lambda_d = 10$. The tracking response of deflection angle and deflection angular velocity under PID control are shown in Figs. 22-23, respectively. Figs. 24-25 display the profiles of deflection angle error and deflection angular velocity error for the case of using PID control law, respectively. By comparing Figs. 22-23 with Figs. 2-3, as well as Figs. 24-25 with Figs. 4-5, we can see that the higher control precision has been achieved for the case of using error-tracking based neuro-adaptive ILC law. Comparing Fig. 16 and Fig. 26, we can see the constraint property observed in the proposed ILC scheme is violated in PID control scheme.

Thus, compared with both PD-type ILC with forgetting factor and PID control, the proposed neuro-adaptive ILC scheme is reasonable for the target of non-uniform trajectory tracking of PAM systems with nonzero initial errors. The above simulation results verify the effectiveness of theoretical analysis in this work.

VII. CONCLUSION

In this paper, for dealing with the non-uniform angle trajectory tracking tasks for PAM systems under nonzero initial errors, high nonlinearities, uncertainties, and time-varying characteristics, an output-constrained error-tracking neuro-adaptive ILC scheme is proposed, which achieves satisfactory accurate tracking control performance. Error-tracking method is used to solve the initial position problem of ILC. A difference-learning neural network is introduced to compensate for the unknown uncertainties in the PAM system. The angle tracking error and angle velocity tracking error can follow the desired error trajectories over the whole time interval as the iteration number increases, which means excellent tracing performance of angle position and angular velocity can be obtained during the preset interval. Moreover, the system output is restrict in the preset bound during system operation. Lyapunov analysis is applied to derive the control law and analyze the stability and learning performance. In addition, the simulation comparison between the proposed control algorithm and two traditional control algorithms, including PID control algorithm and PD-type ILC algorithm are made to verify the effectiveness of the proposed ILC scheme.

REFERENCES

[1] M. Lallart, K. Li, Z. Yang, and W. Wang, "System-level modeling of nonlinear hysteretic piezoelectric actuators in quasi-static operations," *Mech. Syst. Signal Process.*, vol. 116, pp. 985–996, Feb. 2019.
[2] S. Hussain, P. K. Jamwal, M. H. Ghayesh, and S. Q. Xie, "Assist-as-needed control of an intrinsically compliant robotic gait training orthosis," *IEEE Trans. Ind. Electron.*, vol. 64, no. 2, pp. 1675–1685, Feb. 2017.
[3] R. M. Robinson, C. S. Kothera, and N. M. Wereley, "Variable recruitment testing of pneumatic artificial muscles for robotic manipulators," *IEEE/ASME Trans. Mechatronics*, vol. 20, no. 4, pp. 1642–1652, Aug. 2015.
[4] S. Dirven and A. McDaid, "A systematic design strategy for antagonistic joints actuated by artificial muscles," *IEEE/ASME Trans. Mechatronics*, vol. 22, no. 6, pp. 2524–2531, Dec. 2017.
[5] H. Aschemann and D. Schindele, "Sliding-mode control of a high-speed linear axis driven by pneumatic muscle actuators," *IEEE Trans. Ind. Electron.*, vol. 55, no. 11, pp. 3855–3864, Nov. 2008.
[6] Y. Chen, N. Sun, D. Liang, Y. Qin, and Y. Fang, "A neuroadaptive control method for pneumatic artificial muscle systems with hardware experiments," *Mech. Syst. Signal Process.*, vol. 146, Jan. 2021, Art. no. 106976.
[7] N. Sun, D. Liang, Y. Wu, Y. Chen, Y. Qin, and Y. Fang, "Adaptive control for pneumatic artificial muscle systems with parametric uncertainties and unidirectional input constraints," *IEEE Trans. Ind. Informat.*, vol. 16, no. 2, pp. 969–979, Feb. 2020.
[8] J. Huang, J. Qian, L. Liu, Y. Wang, C. Xiong, and S. Ri, "Echo state network based predictive control with particle swarm optimization for pneumatic muscle actuator," *J. Franklin Inst.*, vol. 353, no. 12, pp. 2761–2782, Aug. 2016.
[9] T. Leephakpreeda, "Fuzzy logic based PWM control and neural controlled-variable estimation of pneumatic artificial muscle actuators," *Expert Syst. Appl.*, vol. 38, no. 6, pp. 7837–7850, Jun. 2011.
[10] L. Zhao, H. Cheng, Y. Xia, and B. Liu, "Angle tracking adaptive backstepping control for a mechanism of pneumatic muscle actuators via an AESO," *IEEE Trans. Ind. Electron.*, vol. 66, no. 6, pp. 4566–4576, Jun. 2019.
[11] Y. Yuan, Y. Yu, and L. Guo, "Nonlinear active disturbance rejection control for the pneumatic muscle actuators with discrete-time measurements," *IEEE Trans. Ind. Electron.*, vol. 66, no. 3, pp. 2044–2053, Mar. 2019.
[12] S. Arimoto, S. Kawamura, and F. Miyazaki, "Bettering operation of robots by learning," *J. Robotic Syst.*, vol. 1, no. 2, pp. 123–140, Jun. 1984.
[13] S.-R. Oh, Z. Bien, and I. H. Suh, "An iterative learning control method with application to robot manipulators," *IEEE J. Robot. Autom.*, vol. 4, no. 5, pp. 508–514, Oct. 1988.
[14] A. Tayebi, S. Abdul, M. B. Zaremba, and Y. Ye, "Robust iterative learning control design: Application to a robot manipulator," *IEEE/ASME Trans. Mechatronics*, vol. 13, no. 5, pp. 608–613, Oct. 2008.
[15] F. Bouakrif and M. Zasadzinski, "High order iterative learning control to solve the trajectory tracking problem for robot manipulators using Lyapunov theory," *Trans. Inst. Meas. Control*, vol. 40, no. 15, pp. 4105–4114, Nov. 2018.
[16] S. S. Saab, W. G. Vogt, and M. H. Mickle, "Learning control algorithms for tracking 'slowly' varying trajectories," *IEEE Trans. Syst., Man, Cybern., B, Cybern.*, vol. 27, no. 4, pp. 657–670, Aug. 1997.
[17] J.-X. Xu and J. Xu, "On iterative learning from different tracking tasks in the presence of time-varying uncertainties," *IEEE Trans. Syst., Man Cybern., B, Cybern.*, vol. 34, no. 1, pp. 589–597, Feb. 2004.

[18] X.-D. Li, M.-M. Lv, and J. K. L. Ho, "Adaptive ILC algorithms of nonlinear continuous systems with non-parametric uncertainties for non-repetitive trajectory tracking," *Int. J. Syst. Sci.*, vol. 47, no. 10, pp. 2279–2289, Jul. 2016.
[19] C.-J. Chien, "A combined adaptive law for fuzzy iterative learning control of nonlinear systems with varying control tasks," *IEEE Trans. Fuzzy Syst.*, vol. 16, no. 1, pp. 40–51, Feb. 2008.
[20] Q. Z. Yan, M. X. Sun, and J. P. Cai, "Reference-signal rectifying method of iterative learning control," *Acta Autom. Sinica*, vol. 43, no. 8, pp. 1470–1477, Aug. 2017.
[21] Q. Yan and M. Sun, "Error-tracking iterative learning control with state constrained for nonparametric uncertain systems," *Control Theory Appl.*, vol. 32, no. 7, pp. 895–901, 2015.
[22] Q. Ai, D. Ke, J. Zuo, W. Meng, Q. Liu, Z. Zhang, and S. Q. Xie, "High-order model-free adaptive iterative learning control of pneumatic artificial muscle with enhanced convergence," *IEEE Trans. Ind. Electron.*, vol. 67, no. 11, pp. 9548–9559, Nov. 2020.
[23] M. Burger and M. Guay, "Robust constraint satisfaction for continuous-time nonlinear systems in strict feedback form," *IEEE Trans. Autom. Control*, vol. 55, no. 11, pp. 2597–2601, Nov. 2010.
[24] K. Zhang, C. Liu, and Y. Shi, "Self-triggered adaptive model predictive control of constrained nonlinear systems: A min-max approach," *Automatica*, vol. 142, Aug. 2022, Art. no. 110424.
[25] N. Li, I. V. Kolmanovsky, and A. Girard, "A reference governor for nonlinear systems with disturbance inputs based on logarithmic norms and quadratic programming," *IEEE Trans. Autom. Control*, vol. 65, no. 7, pp. 3207–3214, Jul. 2020.
[26] K. P. Tee, S. S. Ge, and E. H. Tay, "Barrier Lyapunov functions for the control of output-constrained nonlinear systems," *Automatica*, vol. 45, no. 4, pp. 918–927, Apr. 2009.
[27] S. Xie, M. Tao, Q. Chen, and L. Tao, "Neural-network-based adaptive finite-time output constraint control for rigid spacecrafts," *Int. J. Robust Nonlinear Control*, vol. 32, no. 5, pp. 2983–3000, Mar. 2022.
[28] J. Zhang, S. Li, C. K. Ahn, and Z. Xiang, "Adaptive fuzzy decentralized dynamic surface control for switched large-scale nonlinear systems with full-state constraints," *IEEE Trans. Cybern.*, vol. 52, no. 10, pp. 10761–10772, Oct. 2022.
[29] X. Guan, Z. He, M. Zhang, and H. Xia, "Filtering-error constrained angle tracking adaptive learning fuzzy control for pneumatic artificial muscle systems under nonzero initial errors," *IEEE Access*, vol. 10, pp. 41828–41838, 2022.
[30] Y. Sun, P. Xia, and H. Lin, "Iterative learning control for a class of nonlinear batch processes with state delay," *J. Syst. Eng. Electron.*, vol. 33, no. 2, pp. 380–384, 2011.

GUANGMING ZHU received the B.S. degree in computer science and technology and the M.S. degree in computer science from Hangzhou Dianzi University, Hangzhou, in 2011 and 2016, respectively. He is currently an Instructor of experiment with the Zhejiang University of Water Resources and Electric Power. His research interests include computer numerical control and adaptive learning control.

QIUZHEN YAN received the M.S. degree in computer science and the Ph.D. degree in control science and engineering from the Zhejiang University of Technology, Hangzhou, China, in 2005 and 2015, respectively. He is currently an Associate Professor with the College of Information Engineering, Zhejiang University of Water Resources and Electric Power. His research interests include iterative learning control and repetitive control. He is a Senior Member of the Chinese Association of Automation.